Exciting cytoskeleton-membrane waves

R. Shlomovitz and N. S. Gov
Department of Chemical Physics, The Weizmann Institute of Science, P. O. Box 26, Rehovot, Israel 76100
(Received 30 July 2008; published 17 October 2008)

Propagating waves on the surface of cells, over many micrometers, involve active forces. We investigate here the mechanical excitation of such waves when the membrane is perturbed by an external oscillatory force. The external perturbation may trigger the propagation of such waves away from the force application. This scheme is then suggested as a method to probe the properties of the excitable medium of the cell, and learn about the mechanisms that drive the wave propagation. We then apply these ideas to a specific model of active cellular membrane waves, demonstrating how the response of the system to the external perturbation depends on the properties of the model. The most outstanding feature that we find is that the excited waves exhibit a resonance phenomenon at the frequency corresponding to the tendency of the system to develop a linear instability. Mechanical excitation of membrane waves in cells at different frequencies can therefore be used to characterize the properties of the mechanism underlying the existence of these waves.

DOI: 10.1103/PhysRevE.78.041911 PACS number(s): 87.16.D−, 05.60.−k, 87.16.A−, 87.16.Uv

I. INTRODUCTION

Recently, there has been a growing number of observations of membrane waves and ruffles that propagate over the surface of living cells [1–6]. One of the outstanding properties of these waves is that they propagate without significant damping over a large portion of the cell surface, i.e., up to tens of micrometers. This feature in a highly damped viscous system indicates that there are active forces involved in driving these waves over such long distances. Such active forces can arise in cell membranes from ion pumps and channels [7], and from the cytoskeleton underlying the membrane [3,8].

In this paper we suggest several experiments that may be used to study the excitation mechanism of such waves, and test the validity of various quantitative theoretical models. We describe the mechanical excitation of membrane waves using an oscillating force applied to the membrane. This force application can be in different forms (Fig. 1); the oscillating tip of an atomic force microscope (AFM) [9], a thin micropipette [10], an attached magnetic bead [11,12], a magnetic microneedle [13], or optical tweezers [14]. We calculate the resulting waves triggered by such a mechanical perturbation of the cell, using our model of cytoskeleton-membrane waves [15], as an example. Using these calculated waves we give several predictions that can be used to experimentally test the validity of the theoretical models.

Existing experimental works that investigated the mechanical response of cells to an applied force have mostly dealt with the behavior of the bulk of the cytoskeleton. These experiments have found that the cells behave as a soft gel, with unusual properties such as a multitude of relaxation time scales ("soft glass") [16], and used a variety of probes such as magnetic beads attached to the cell [17] or engulfed by the cell [18]. These probes usually have a diameter of order $1-2\ \mu$m. In this work we wish to propose experiments that probe in a highly localized manner the cell membrane and the cortical cytoskeleton in the thin layer (up to $1\ \mu$m) underneath the membrane. Specifically, we are interested in cells that have been shown to support propagating cytoskeleton-membrane waves in certain parts of their membrane, such as in the lamellipodia or in spreading cells. This regime has not been investigated experimentally so far, and our calculations are aimed at encouraging such experiments with the purpose of exciting such waves mechanically and studying their properties.

In Sec. II we calculate the waves triggered by a normal mechanical perturbation of the membrane using our cytoskeleton-membrane wave model. In Sec. III we discuss several testable predictions that can be used to quantitatively study the properties of such excited waves. The reader who is not interested in the details of our particular wave model can skip Sec. II.

II. EXCITATION OF WAVES IN PLANAR AND ROTATIONAL SYMMETRY

In this section we calculate the waves that can be triggered in an active cortical cytoskeleton due to a mechanical perturbation of the membrane. We assume in this calculation that the cortical cytoskeleton is in a state of a high level of actin polymerization activity and treadmilling, so that it can rearrange on a relatively short time scale. This means that

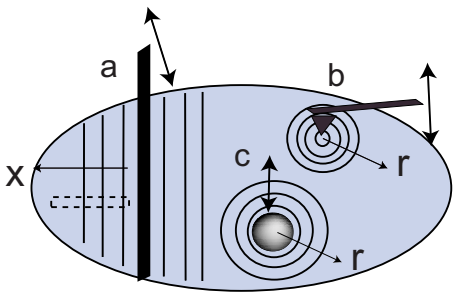

FIG. 1. (Color online) Illustration of the proposed mechanical excitation of membrane waves on cells, by applying an oscillatory normal force using (a) a thin pipette (planar waves), or (b) an AFM tip and (c) bead (magnetic or optical tweezers), producing circular waves.

during slow perturbations (frequency $\omega < 1$ Hz) we can describe this medium as an effective viscous fluid. We consider here cells that are adhering and well spread over a flat substrate (nonmotile) [3]. Furthermore, the force application is considered in a region where the membrane is rather flat. The mechanical perturbation triggers the response of the active cortical cytoskeleton due to the imposed changes in the local membrane curvature. The energy supplied to the system through the mechanical perturbation is very small, while the waves that propagate in the active cytoskeleton are driven by forces produced due to ATP consumption in the cell (actin polymerization and myosin contraction).

In Fig. 1 we show schematically several possibilities of applying an oscillatory force to the cell membrane, which can be divided into those that produce a force along a line and at a point (approximately). We therefore calculate below the waves that are produced in these two geometries, planar and polar respectively. In both cases we solve the equations of motion of the coupled membrane-actin-myosin system [15], where we impose an oscillating force at the origin,

$$\frac{\partial h}{\partial t} = \hat{\mathcal{O}}\left(-\kappa\nabla^4 h + \sigma\nabla^2 h - \gamma h + \frac{\kappa\bar{H}}{n_0}\nabla^2 n - A^* m + An + f_0 e^{i\omega_0 t}\delta(r)\right), \tag{1}$$

$$\frac{\partial m}{\partial t} = -k_{\text{off}} m + k_{\text{on}} n, \tag{2}$$

$$\frac{\partial n}{\partial t} = D\nabla^2 n - \Lambda\kappa\bar{H}\nabla^4 h, \tag{3}$$

where h is the local normal deformation of the membrane from flatness, n is the local density of actin nucleating proteins, m is the local density of myosin motors attached to the actin filaments, κ and σ are the membrane bending modulus and tension respectively, $A(A^*)$ is the actin (myosin) protrusive (contractile) force coefficient, D is the diffusion coefficient of the actin nucleating proteins, k_{on}, k_{off} are the myosin-actin binding-unbinding rate parameters, $\Lambda = D/k_B T$, and $\bar{H}$ is the spontaneous curvature of the actin nucleators. In our scheme m represents myosins that are attached to actin filaments, and therefore are recruited only where n exists. The reader is referred to [15] for more details of this model. A local elastic restoring force, with spring constant proportional to γ, is added to mimic the passive component of the elastic cytoskeleton gel beneath the membrane, in the form of a Hookean force term in the equation of motion of the membrane [Eq. (1)]. This term describes a layer of springs that are not connected laterally, which describes oscillations of an elastic layer with a wavelength that is much larger than the width of the layer.

The oscillating force is represented by Dirac's delta function $\delta(r)$, where ω_0 is the driving frequency and f_0 is the amplitude. We assume here a local version of the hydrodynamic interaction kernel ($\hat{\mathcal{O}}$) and of the myosin-induced kernel force, and neglect any sources of noise [15]. The membrane flux of proteins n is defined from Eq. (3): $\partial n/\partial t \equiv -\nabla \cdot J_n \Rightarrow J_n = -D\partial n/\partial x + \Lambda\kappa\bar{H}\partial^3 h/\partial x^3$.

In Figs. 2(a)–2(c) we plot the dispersion relation $\omega(q)$ for the oscillatory mode [15], where we compare it to the dispersion of a passive membrane, with and without the elastic spring term. Note that there are three modes in this system, corresponding to three dynamic variables [15]; two modes that are complex conjugate of each other in the range of q's that give waves [$q < q_\omega$ shown in Figs. 2(a)–2(c)], and another mode that is negative and real for all q's and therefore represents a damped mode which is not of interest here. The passive membrane is described by decoupling the membrane from the forces of the cytoskeleton, i.e., Eq. (1) without the n- and m- dependent terms. Note that the wave velocity of the active membrane is given by the slope of the imaginary part $\omega''(q)$ [Fig. 2(b)], which is not strongly affected by the elastic spring term. For wave vectors larger than q_ω there are no oscillatory modes [Fig. 2(c)]. We chose the parameters of the system to be those that gave the best fit to a particular kind of cellular membrane wave [1,15]. The dispersion relation for this system has a subcritical point at the wave vector $q_{\max} = 27\sqrt{A^*|H|k_{\text{on}}\kappa\Lambda\hat{\mathcal{O}}}/8D^{3/2}$, at which the real part of the dispersion relation of the system has an extremum (for $q > 0$). At this wave vector the waves have the frequency $\omega_{\max} \simeq v q_{\max}$ [Fig. 2(b)], where v is the velocity of the actin-myosin-membrane waves [Eq. (7)], which is the slope of $\omega''(q)$ for small q's [Fig. 2(c)].

The system of equations (1)–(3) can be shown to give rise to propagating waves, as follows: in the limit of strong myosin contractility and strong myosin adsorption to actin, we can simplify Eqs. (1) and (2) by (neglecting the driving term)

$$\frac{\partial h}{\partial t} \approx -\hat{\mathcal{O}} A^* m, \tag{4}$$

$$\frac{\partial m}{\partial t} \approx k_{\text{on}} n. \tag{5}$$

Substituting Eq. (4) in Eq. (5), we have a relation between h and n, which we then substitute into Eq. (3), after differentiating twice with respect to time, to get

$$\ddot{n} = D\nabla^2 \ddot{n} + \hat{\mathcal{O}} k_{\text{on}} A^* \Lambda\kappa\bar{H}\nabla^4 n. \tag{6}$$

In the limit of $qv > w$ we can neglect the left-hand side and recover the familiar form of a wave equation for $\bar{H} < 0$, with solutions in the form $\cos(\omega t - qvx)$, where the wave velocity is

$$v = \sqrt{k_{\text{on}} A^* \Lambda\kappa|\bar{H}|\hat{\mathcal{O}}/D}. \tag{7}$$

Note that in this model the roles of the actin and myosin (n and m, respectively) cannot be replaced by a single parameter which is either protrusive or contractile alone, since it is the different dynamics of these two opposing forces that gives rise to the propagating wave.

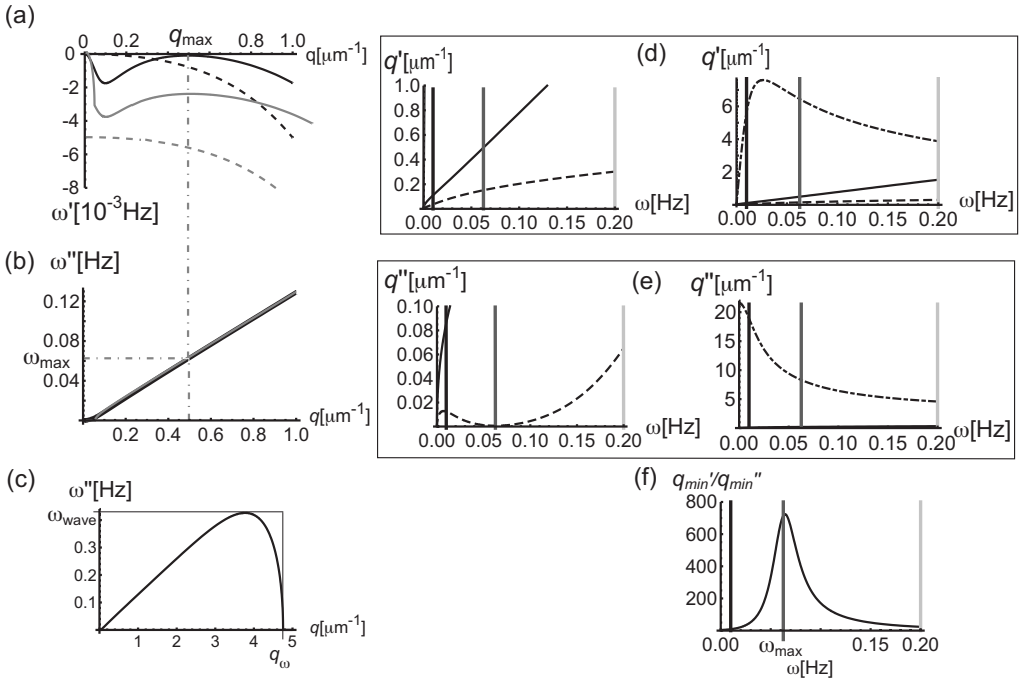

FIG. 2. (a)–(c) Dispersion relation of the active membrane model [15]. (a) The real part of the dispersion $\omega'(q)$ of the active membrane is shown compared to the response of a passive membrane (dashed lines). Black and gray correspond to $\gamma=0,4k_BT/\mu m^4$, respectively. We indicate the wave vector $q_{\max}$ where the dispersion of the active membrane has an extremum. (b) The imaginary (oscillatory) part of the dispersion $\omega''(q)$, where we indicate the value of $\omega_{\max}$. (c) Same as (b) on a larger scale to indicate the range of frequencies and wave vectors for which the active membrane supports oscillatory modes. (d) Real part of the wave vectors $q_{1,2,3}$ that are excited in the active membrane by the application of a force at frequency ω. The vertical lines indicate three typical frequencies below, at, and above the resonance frequency $\omega_{\max}$, which we use in Fig. 3. (e) Same as (d) for the imaginary part of the wave vectors $q_{1,2,3}$. The dashed line indicates the wave vector which has a distinct minimum, and is denoted by $q_{\min}$. (f) Ratio of $q'_{\min}/q''_{\min}$ that gives the number of wavelengths before there is significant decay (damping) of the waves.

A. Excitation of waves from an oscillating linear source; planar waves

Excitation of waves on a planar membrane along a line parallel to the y axis [Fig. 1(a)], reduces the problem to one-dimensional waves propagating in the x direction. We solve these equations using the linear response method [19], for the limit of long times, such that the transient response of the system has already decayed. We Fourier transform the set of equations (1)–(3), to get the following equations in a matrix form:

$$(M+i\omega I)\begin{pmatrix} h(q,\omega) \\ m(q,\omega) \\ n(q,\omega) \end{pmatrix} = \begin{pmatrix} f_0\delta(\omega-\omega_0) \\ 0 \\ 0 \end{pmatrix}, \tag{8}$$

$$M = \begin{pmatrix} \hat{O}(-\kappa q^4-\sigma q^2-\gamma) & -\hat{O}A^* & \hat{O}(A-\kappa\bar{H}q^2/n_0) \\ 0 & -k_{\rm off} & k_{\rm on} \\ -\Lambda\kappa\bar{H}q^4 & 0 & -Dq^2 \end{pmatrix},$$

where I is the identity matrix. Fourier transforming the solution back to the time coordinate, we get

$$\begin{pmatrix} h(q,t) \\ m(q,t) \\ n(q,t) \end{pmatrix} = \frac{M'}{\det(M+i\omega_0 I)}\begin{pmatrix} f_0 e^{i\omega_0 t} \\ 0 \\ 0 \end{pmatrix}, \tag{9}$$

where M' is given by $M'=\det(M+i\omega_0 I)(M+i\omega_0 I)^{-1}$. The Fourier transform back to the x space is done using complex analysis, where for positive x we sum the residues of the singularities at $q_{1,2,3}$ that are the solutions of the equation $\det(M+i\omega_0 I)=0$ in the upper half plane, which we plot in Figs. 2(d) and 2(e). We then get

$$\begin{pmatrix} h(x,t) \\ m(x,t) \\ n(x,t) \end{pmatrix} = \sum_{\substack{j=1,2,3 \\ q=q_j}} \frac{iM'}{\det(M+i\omega_0 I)}\begin{pmatrix} f_0 e^{i(q_j x+\omega_0 t)} \\ 0 \\ 0 \end{pmatrix}. \tag{10}$$

We give the explicit expressions for these solutions in the Appendix. Note that the solution we derive by the above procedure of Fourier transform satisfies the boundary conditions of $h,m,n=0$ at $x=\pm\infty$, $\partial h/\partial x=0$ at $x=0$, and $J_n=0$ at $x=0$. Since the membrane waves are excited at the driving frequency, we have $\omega=\omega_0$ in the rest of the paper.

B. Excitation of waves from an oscillating point source; circular waves

We next calculate the waves that are excited in a flat membrane from a point force source at the origin. In this

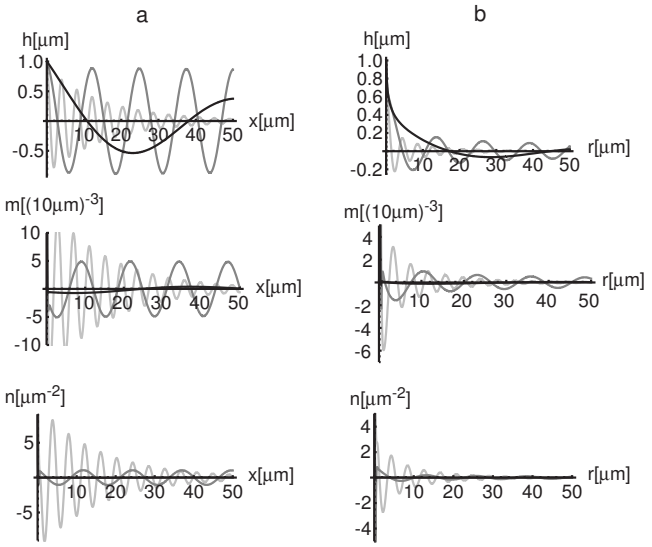

FIG. 3. (a),(b) Calculated membrane height and myosin and actin densities as a function of position, for planar and circular waves, respectively. The black, gray, and light gray lines indicate different frequencies, given in Figs. 2(d)–2(f). The waves close to the resonance frequency (gray lines) have the slowest decay, compared to larger and smaller frequencies (light gray and black lines, respectively). The circular waves (b) decay faster from the origin due to the circular geometry, compared to the planar waves (a).

case we write our equations of motion (1)–(3) in polar coordinates, such that the second spatial derivative is replaced by the radial part of the Laplacian in polar symmetry, and the fourth spatial derivative is replaced by the radial part of a bi-Laplacian.

We solve the equations again using the Fourier transform technique. The solutions we find have the form given in the Appendix for the planar case, simply by replacing $e^{iq_{1,2,3}|x|}/q_{1,2,3} \rightarrow H_0^{(1)}(q_{1,2,3}r)$, where $H_0^{(1)}(qr)=J_0(qr)+iY_0(qr)$ is the Hankel function of the first kind, and $J_0(qr)$, $Y_0(qr)$ are the Bessel functions of the first and second kinds. These solutions satisfy the boundary conditions of zero current $J_n=0$ at the origin, extremum of the amplitude of h at the origin, and vanishing amplitudes at infinity. Note that the Bessel functions $J_0(qr)$ and $Y_0(qr)$ behave at large r as $\sqrt{2/(\pi qr)}\cos(qr)$ and $\sqrt{2/(\pi qr)}\sin(qr)$, respectively. For a complex q both of these functions diverge at $r \rightarrow \infty$, which is the reason that we chose to use the Hankel function, which vanishes at $r \rightarrow \infty$, when doing the reverse Bessel-Fourier (Hankel) transform back into real space.

The solutions for the concentrations of the myosin m, and the membranal protein n diverge at $r \rightarrow 0$, but since the divergence varies as $\log(r)$ and the area element at the origin varies as $r\,dr\,d\theta$, the number of proteins at the origin vanishes.

C. Discussion

In Figs. 3(a) and 3(b), we plot the solutions for the membrane height amplitude, and myosin and actin densities (h, m, and n, respectively), as a function of the position away from the excitation source, for both the planar [Fig. 3(a)] and circular waves [Fig. 3(b)], at a given time. Note that the plots are for different frequencies and we normalized the membrane amplitude by the maximal value at the origin, since it diverges as $|h(0)| \propto 1/\omega$ for $\omega \rightarrow 0$.

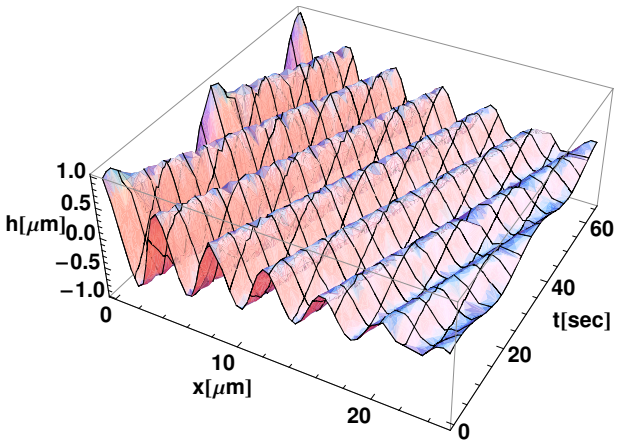

FIG. 4. (Color online) Calculated membrane height amplitude as a function of space and time, $h(x,t)$, for a planar wave at a frequency of $\omega=0.2$ Hz, along an orthogonal line that extends from the force application point [dashed rectangle in Fig. 1(a)]. The waves are shown to propagate away from the source of excitation.

We see in Figs. 3(a) and 3(b) that the waves decay away from the excitation point, with a decay length that strongly depends on the frequency. The amplitude of the membrane height and density oscillations is given by the sum of the contributions of the three modes, as given in Eq. (10) for example. The amplitude of each of these modes $q_{1,2,3}$ decays away from the force excitation point as $\exp[-q''(\omega)x]$, where $q''(\omega)$ is the imaginary part of $q(\omega)$ shown in Fig. 2(e). For our system we find that one of the modes has a very small value of $q''(\omega)$ at $\omega_{\max}$, and we denote this mode as $q_{\min}$. The reason for the small value of $q''(\omega)$ at $\omega_{\max}$ can be seen in Figs. 2(a) and 2(b), where at this frequency the dispersion relation has a very small real part corresponding to very weak damping. It is clear from Figs. 3(a) and 3(b) that the excited waves decay over the longest distance at this resonance frequency $\omega_{\max}$ due to the small value of $q''_{\min}(\omega)$ at that frequency. Note that the waves in the circular geometry [Fig. 3(b)] decay faster compared to the planar waves [Fig. 3(a)], making the experimental distinction between the different frequencies harder to measure in this geometry.

In Fig. 2(f) we plot the ratio of $q'_{\min}/q''_{\min}(\omega)$, which gives the number of wavelengths before there is significant decay (damping) of the waves, as a function of the frequency. The frequency that corresponds to the maximum of this graph is close to $\omega_{\max}$ [gray vertical line in Fig. 2(f)].

In Fig. 4 we plot the membrane height amplitude as a function of space and time $h(x,t)$ for a planar wave, to illustrate the outward propagation of the waves from the line of force application at the origin, i.e., the x axis is orthogonal to the line of force application [dashed rectangle in Fig. 1(a)].

To summarize this section, we find that our model of cytoskeleton-membrane waves [15] gives rise to propagating waves when the membrane is excited by the application of an oscillatory vertical force [Figs. 3(a), 3(b), and 4]. Further-

more, these waves have a resonancelike effect, where they are very weakly damped [Fig. 2(f)].

III. EXPERIMENTAL TESTS OF THE PROPERTIES OF EXCITED WAVES

In this section we give several quantitative measurements that can be used to test the properties of excited cell membrane waves, using the setup of Fig. 1. We will use the calculated waves of the previous section to demonstrate the proposed measurements.

The simplest prediction is just to measure the membrane height amplitude as a function of the spatial distance from the point of force application, and as a function of time, i.e., $h(x,t)$ (Fig. 4). This measurement might be difficult to perform if the membrane height amplitude is small [3], or decays over a short distance. We therefore suggest another experiment, where the height amplitude of a small marker (for example a small fluorescent bead) is measured with high resolution, at a fixed distance X from the point of force application, as a function of the frequency. In Fig. 5 we plot the ratio $h_{\max}(X)/h_{\max}(0)$ of the amplitude of the membrane oscillation at a distance of $X=0.3$ μm [Fig. 5(a)] and $X=5$ μm [Fig. 5(b)], as a function of frequency. We find that the amplitude of the (damped) oscillations of a passive membrane at $X=0.3$ μm monotonically decays as a function of the frequency (for planar geometry). At this distance the active waves (Sec. II) have a larger amplitude, which remains almost constant up to frequencies of order ω_{wave} [Fig. 2(c)]. At a larger distance of $X=5$ μm [Fig. 5(b)] the amplitude of the passive membrane becomes negligibly small, while the amplitude of the active waves is still significant, and has a local maximaum around the resonance frequency which becomes more pronounced as the distance X is increased. In this figure we also show the effect of an elastic spring term which diminishes the amplitude of the waves. The dependence of the measured amplitude on the driving frequency could therefore provide a useful method for distinguishing between the contribution of the active waves, and the passive response of a membrane coupled to a viscoelastic medium.

An experiment that has probed the fluctuations of a membrane probe due to an applied oscillatory force is described in [17]. In these experiments a large bead of 2 μm diameter was used to apply a torque to the cell cytoskeleton and membrane at a frequency of 1.3 Hz, while a small fluorescent probe at 7–8 μm away was monitored. The results showed some dependence of the amplitude of the probe on the magnitude of the applied force, and found that beyond a distance of 10–15 μm there was no measurable displacement of the probe. Although these experiments are not exactly in the regime where a localized normal force (not a torque) is applied to a cell which supports waves, these results may nevertheless be compared to our calculations shown in Figs. 3(a) and 3(b) and Figs. 5(a) and 5(b) where we calculate the damping of the waves as a function of the distance from the force center, and as a function of frequency. Such experiments could be used in the future to test these predictions.

Another measurement that probes the response properties of the membrane, is the phase lag between the force application and the motion of the membrane at the same point. This could be measured by observing the motion of a fluorescent bead which is also used as the force application instrument (by magnetic field or optical tweezers). From our model of Sec. II we can plot the dependence of this phase lag as a function of the frequency, as shown in Fig. 5(c). We find that for our active waves model, without an elastic term $\gamma=0$ (solid black line), the phase lag starts at a value of $-\pi/4$ for $\omega\to 0$, then has a maximum at $\omega_{\max}$ with a value which is close to $-\pi/16$, and finally approaches $-3\pi/8$ for $\omega\to\infty$. The value at $\omega\to\infty$ is simply the behavior of a passive membrane dominated by the restoring force of the curvature [first term in Eq. (1)] shown by the dashed black line. The value of $-\pi/4$ at $\omega\to 0$ arises from the behavior of a damped oscillator when the restoring force vanishes linearly with the frequency, which is the behavior of the passive membrane in

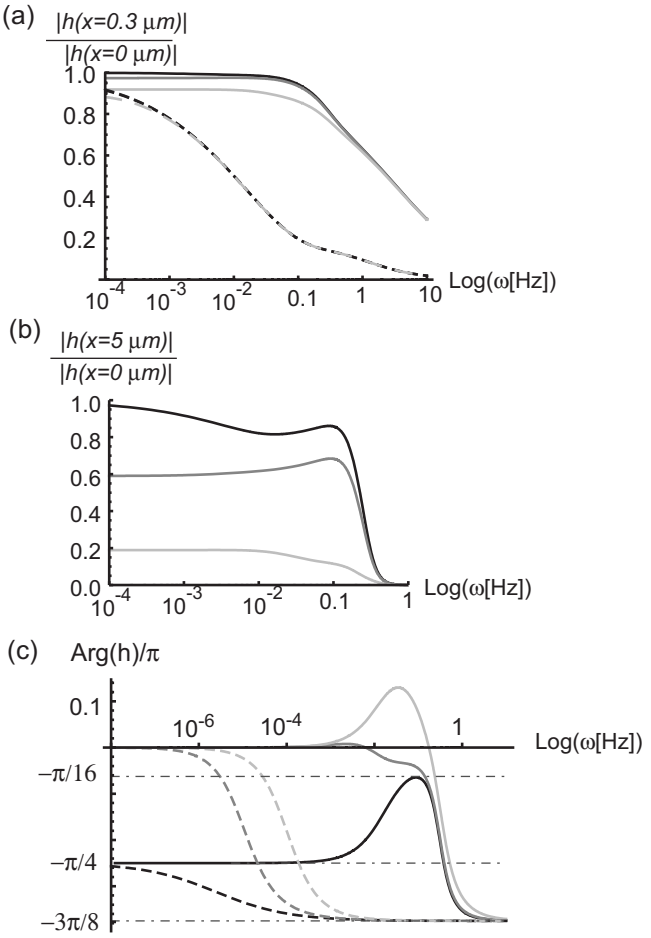

FIG. 5. (a) Calculated ratio $h_{\max}(X)/h_{\max}(0)$ of the amplitude of the membrane oscillation at a distance of $X=0.3$ μm, as a function of the frequency. Black, gray, and light gray correspond to $\gamma=(0,2,20)k_BT/\mu\text{m}^4$, respectively. Dashed line gives the amplitude of an excited passive membrane. (b) Same as in (a) but for a location at $X=5$ μm, with the same color scheme. At this location the amplitude of the passive membrane fluctuations are too small to plot. (c) Calculated phase lag between the applied force and the membrane motion at the origin, for the active (solid lines) and the passive membrane (dashed lines). The color scheme indicates the values of γ as in (a),(b).

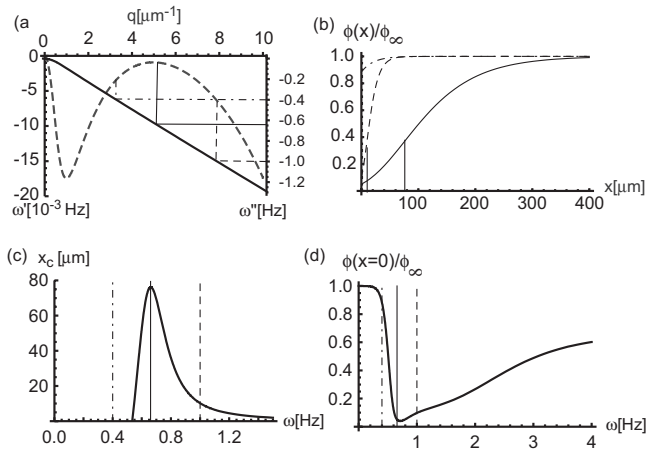

FIG. 6. (a) Dispersion relation of the active membrane model [15] used for the calculation of the wave-induced density hole. Heavy solid (dashed) line gives $\omega''(q)$ [$\omega'(q)$]. (b) Calculated steady-state density profiles of the membrane markers, as a function of the distance x from the wave excitation source. The solid, dashed, and dash-dotted lines correspond to excitation frequencies $\omega=0.66,1,0.4$Hz respectively. The vertical lines indicate the distance to the inflection point, which we denote by x_c. The dependence of x_c, the estimated size of the hole, is plotted in (c) as a function of the frequency [Eq. (11)]. (d) The depth of the depletion hole at the origin plotted as a function of the frequency. In both (c) and (d) we find that the most pronounced hole appears around the resonance frequency, which correspond to the smallest damping [$\omega'(q)$, dashed line in (a)]. The vertical lines in (c),(d) correspond to the frequencies indicated in (a),(b) by the same notation.

this limit, dominated by membrane tension [second term in Eq. (1)].

The elastic spring term is seen to shift the phase lag at small frequencies to zero, while the limit at $\omega\to\infty$ stays unchanged [Fig. 5(c)]. The solid gray line shows that for certain values of γ the distinct peak in the phase lag of the active membrane, around the resonance frequency, may vanish, making the curve similar in shape to the passive membrane. An experimental measurement of the phase lag for a torque application to the cell membrane and cytoskeleton [20] found a small phase lag which is almost independent of the frequency, up to $\sim$100–1000 Hz. This behavior is typical for a viscoelastic medium, where the elastic part is represented in our model by the spring constant γ. These experiments do not probe the regime of membrane-cytoskeleton waves that we are interested in, and indeed at high frequencies the response that was measured was not dominated by the bending modulus of the membrane, as we calculated here [Fig. 5(c)]. High-frequency modes of the membrane correspond to short wavelengths, which are not probed in these experiments that use a large bead for the force induction (diameter of 2 μm), and therefore probe the bulk properties of the cytoskeleton while being not very sensitive to the membrane properties, which we focus on.

Finally, in Fig. 6 we demonstrate the effect of mechanically excited membrane waves on the spatial distribution of freely diffusing membranal markers that have a spontaneous curvature. The theoretical description of this effect is given in [8], where we show that propagating membrane waves can cause a flow of curved membrane markers away from the source of the waves, resulting in a local depletion of the markers density close to the origin ("hole"). Using the parameters of the wave model that we used for the calculations above [dispersion relation of Figs. 2(a) and 2(b)], there is no significant motion of the markers due to the waves (for realistic values of the markers' properties; see below). The reason is that these waves have a very large wavelength at the resonance $2\pi/q_{\max}\sim 12$ μm, which results in a very small drift force [8]. For this reason we illustrate below the formation of a significant density "hole," using modified cytoskeleton-membrane waves with a resonance wavelength of ~ 1 μm with the same velocity as before, given by the dispersion relation shown in Fig. 6(a). Membrane waves and ruffles with similar properties are observed in cells [2,3], and therefore these are reasonable values.

As in [8], we assume that the wave-induced flow of the proteins at each position x away from the wave initiation point is given by the drift velocity calculated for a wave of uniform amplitude, where the amplitude corresponding to this distance x is given by Eq. (10). In our case we have a sum of three waves that each have an exponential decay. The dominant contribution comes from the wave with the slowest decay, i.e., with $q_{\min}$, which is the only wave we keep in the calculation below; $h(x,t)=\exp-(q''_{\min}x)\sin(q'_{\min}x-\omega t)$. We use this decaying wave in the approximate calculation of the steady-state density profile of the membrane proteins [8], as shown in Fig. 6.

Following [8], we can estimate the size of the depletion hole to be

$$x_c=\frac{1}{2\alpha}\ln\left(\frac{\varepsilon^2}{4\alpha[(D_m/v)^3q'^2_{\min}+(D_m/v)]}\right), \qquad (11)$$

where $\alpha=q''^{-1}_{\min}$ is the exponential decay length of the waves away from the initiation site, $v=q'_{\min}/\omega$ is the wave velocity, and ε is the ratio of the drift to the wave velocity at the origin; $\varepsilon=|q'_{\min}|^3\kappa\Lambda_m\bar{H}_m h_0 a^2/v$, where $\kappa=10k_BT$, $\Lambda_m=D_m/k_BT$, $D_m=0.1$ μm^2/s is the diffusion coefficient of the markers, $\bar{H}_m=100$ μm^{-1} is the spontaneous curvature of the markers, $h_0=0.1$ μm is the amplitude of the membrane oscillation at the origin, and $a\sim 10$ nm is the diameter of the membrane marker. Note that we change the amplitude of the applied oscillatory force, so that the waves are excited with a constant amplitude at the origin h_0, independent of ω, as given in Eq. (15).

We plot in Fig. 6(c) the calculated dependence of the size of the depletion hole x_c [Eq. (11)] on the driving frequency. Our results show that the size of the hole is maximal at the resonance frequency $\omega_{\max}$, provided that the ratio between the curvature-induced flow velocity and the wave velocity $\varepsilon=v_{\text{drift}}/v$ is larger than 1, so that at least close to the force initiation site the membrane proteins can "surf" with the excited waves [8]. The density profiles for several frequencies are given in Fig. 6(b), and the depth of the depletion hole at the origin is given in Fig. 6(d). The maximal depletion is again found for the resonance frequency.

The size and depth of the depletion hole as a function of the frequency of the oscillation result from two competing

effects. As the frequency increases, so does the wave vector $q'_{\min}$ and the value of ε at the origin. On the other hand, only close to the resonance frequency is the decay length long (large α), and the waves can induce a drift of the markers over a long distance. The first effect will give rise to strong depletion at the origin for large frequencies, while the second effect will induce a hole of small size at large frequencies. In Fig. 6(a) we indicate the damping $\omega'(q)$ corresponding to each frequency. Specifically, note that, although the damping for $\omega=0.4$ Hz is smaller than for $\omega=1$ Hz, the hole is larger for the latter case due to the larger value of the real part of the wave vector q (x axis) and therefore the drift velocity.

IV. CONCLUSION

Propagating waves on the surface of cells involve active forces and result in a traveling undulation of the membrane. We propose here that such waves should therefore be mechanically excited when the membrane is perturbed by an external oscillatory force. The external perturbation may trigger the propagation of such waves away from the force application. This scheme is then suggested as a method to probe the properties of the excitable medium of the cell, and learn about the mechanisms that drive the wave propagation.

We then apply these ideas to the specific model of coupled actin–myosin–cytoskeleton-membrane [15], demonstrating how the response of the system to the external perturbation depends on the properties of the model. The most outstanding feature that we find is that the excited waves exhibit a resonance phenomenon at the frequency corresponding to a subcritical wave vector where the system can develop a linear instability. At this frequency the waves can propagate with very small attenuation over a long distance of many micrometers, as is observed in cells [1–6]. Mechanical excitation of membrane waves in cells at different frequencies can therefore be used to characterize the properties of the mechanisms underlying the existence of these waves.

ACKNOWLEDGMENTS

We thank Ailey Crow for useful comments. We thank the Alvin and Gertrude Levine Career Development Chair, for their support. This research was supported by the Israel Science Foundation (Grant No. 337/05) and by BSF (Grant No. 2006285). This research is made possible in part by the historic generosity of the Harold Perlman family.

APPENDIX

By substituting $q=\sqrt{u}$ in $\det(M+i\omega I)=0$ we get a polynomial of order 3 in u, which has three solutions $u_1(\omega), u_2(\omega), u_3(\omega)$, and six solutions for q: $q_{1,4}=\pm\sqrt{u_1}, q_{2,5}=\pm\sqrt{u_2}, q_{3,6}=\pm\sqrt{u_3}$. While all the solutions have an imaginary part, the three solutions that have a positive imaginary part are denoted as $q_{1,2,3}$, and are the desired ones since we demand that the amplitudes vanish in the limits of $x\to\infty$.

The explicit solutions [Eq. (10)] for the excitation of the membrane along an infinite line at the origin are

$$\begin{pmatrix} h(x,t) \\ m(x,t) \\ n(x,t) \end{pmatrix} = f_0 \pi i e^{i\omega t}\left(\frac{V(q_1)e^{iq_1|x|}}{Cq_1(q_1^2-q_2^2)(q_1^2-q_3^2)} + \frac{V(q_2)e^{iq_2|x|}}{Cq_2(q_2^2-q_1^2)(q_2^2-q_3^2)} + \frac{V(q_3)e^{iq_3|x|}}{Cq_3(q_3^2-q_2^2)(q_3^2-q_1^2)} \right), \tag{A1}$$

where the vector $V(q)$ is given by

$$V(q) = \begin{pmatrix} (k_{\text{off}}+i\omega)(Dq^2+i\omega) \\ -\bar{H}k_{\text{on}}\kappa\Lambda q^4 \\ -\bar{H}\kappa\Lambda q^4(k_{\text{off}}+i\omega) \end{pmatrix} \tag{A2}$$

and $C=\hat{O}\kappa(k_{\text{off}}+i\omega)(Dn_0-\bar{H}^2\kappa\Lambda)/n_0$.

In order to maintain a constant amplitude of the wave at the origin, $|h(0,t)|=h_0$, the amplitude of the force applied has to have the value given by

$$|f_0| = \sqrt{\frac{[Ch_0 q_1 q_2 q_3 (q_1+q_2)(q_2+q_3)(q_3+q_1)]^2}{\pi^2(\omega^2+k_{\text{off}}^2)\{[\omega(q_1+q_2+q_3)]^2+(Dq_1q_2q_3)^2\}}} \tag{A3}$$

which we use in the calculations shown in Fig. 6.

[1] H.-G. Döbereiner, B. J. Dubin-Thaler, J. M. Hofman, H. S. Xenias, T. N. Sims, G. Giannone, M. L. Dustin, C. H. Wiggins, and M. P. Sheetz, Phys. Rev. Lett. **97**, 038102 (2006).
[2] R. B. Buccione, J. D. Orth, and M. A. McNiven, Nat. Rev. Mol. Cell Biol. **5**, 647 (2004).
[3] G. Giannone *et al.*, Cell **128**, 561 (2007).
[4] M. Machacek and G. Danuser, Biophys. J. **90**, 1439 (2005).
[5] J. C. Neto *et al.*, Exp. Cell Res. **303**, 207 (2005).
[6] E. Munro, J. Nance, and J. R. Priess, Dev. Cell **7**, 413 (2004); S. Schonegg *et al.*, Proc. Natl. Acad. Sci. U.S.A. **104**, 14976 (2007); S. Hird, J. Cell. Sci. **109**, 525 (1996).
[7] S. Ramaswamy, J. Toner, and J. Prost, Phys. Rev. Lett. **84**, 3494 (2000).
[8] R. Shlomovitz and N. S. Gov (unpublished).
[9] S. Sen, S. Subramanian and D. E. Discher, Biophys. J. **89**, 3203 (2005).
[10] C. I. Lacayo, Z. Pincus, M. M. van Duijn, C. A. Wilson, D. A. Fletcher, F. B. Gertler, A. Mogilner, and J. A. Theriot, PLoS Biol. **5**, e233 (2007).
[11] M. Puig-De-Morales *et al.*, J. Appl. Physiol. **91**, 1152 (2001).
[12] C. C. Wang, H. J. Jian, C. W. Wu, and C. H. Lee, Microsc. Res. Tech. **71**, 594 (2008).

[13] B. D. Matthews, D. R. Overby, F. J. Alenghat, J. Karavitis, Y. Numaguchi, P. G. Allen, and D. E. Ingber, Biochem. Biophys. Res. Commun. **313**, 758 (2004).
[14] M. Balland, N. Desprat, D. Icard, S. Fereol, A. Asnacios, J. Browaeys, S. Henon, and F. Gallet, Phys. Rev. E **74**, 021911 (2006).
[15] R. Shlomovitz and N. S. Gov, Phys. Rev. Lett. **98**, 168103 (2007).
[16] P. Bursac *et al.*, Nature Mater. **4**, 557 (2005).
[17] T. Ragan, H. Huang, P. So, and E. Gratton, J. Fluoresc. **16**, 325 (2006).
[18] A. R. Bausch, W. Möller, and E. Sackmann, Biophys. J. **76**, 573 (1999).
[19] P. A. Chaikin, and T. C. Lubensky, *Principles of Condensed Matter Physics*, 3rd ed. (Cambridge University Press, Cambridge, U.K., 2006).
[20] L. Deng *et al.*, Nature Mater. **5**, 636 (2006).